

# CORONAS AND IRIDESCENCE IN MOUNTAIN WAVE CLOUDS OVER NORTHEASTERN COLORADO

BY PAUL J. NEIMAN AND JOSEPH A. SHAW

The small, uniformly sized particles in mountain wave clouds give rise to spectacularly colorful optical displays that can be explained with diffraction theory.

The interplay of sunlight, moonlight, or anthropogenic light sources with cloud and precipitation particles can produce a wide variety of optical phenomena, some with dazzling arcs and colors, in the sky around us. These naturally occurring patterns of redistributed light, often referred to generally as atmospheric optics, represent an especially aesthetic component of the field of meteorology. A comprehensive description of natural optical phenomena and their causative mechanisms are provided by Minnaert (1954), Tricker (1970), Greenler (1980), Meinel and Meinel (1983), Minnaert (1992), Tape (1994), and Lynch and Livingston (2001), among others.

Cloud and precipitation particles that produce optical displays are composed of either ice crystals or liquid water drops. Ice crystals are responsible for an incredibly rich palette of halos, arcs, and pillars arising largely from the refraction and/or reflection of light by these crystals. Liquid water particles also produce a variety of optical phenomena, though fewer in number than those arising from ice crystals. Nevertheless, this latter class of displays often exhibits striking color. The most commonly known of these is the rainbow, formed by the refraction and reflection of light by raindrops, creating colored circles of light centered on the point directly opposite the sun or other light source. Equally beautiful are the colorful diffraction patterns caused by light passing through clouds composed of small liquid or ice particles. These patterns are typically referred to as coronas, iridescence, and glories, though this discussion will not include the glories since they are not observed regularly from the ground. Coronas and iridescence are often quite colorful, and they occur rather frequently. However, many are not aware of these diffraction displays during daylight hours because the colors usually remain close to the blinding rays of the sun.

**AFFILIATIONS:** NEIMAN—NOAA/Environmental Technology Laboratory, Boulder, Colorado; SHAW—Montana State University, Bozeman, Montana

**CORRESPONDING AUTHOR:** Paul J. Neiman, NOAA/Environmental Technology Laboratory, 325 Broadway, Boulder, CO 80303  
E-mail: Paul.J.Neiman@noaa.gov  
DOI: 10.1175/BAMS-84-10-1373

In final form 26 February 2003  
© 2003 American Meteorological Society

Coronas and iridescence are two closely related types of colorful displays in clouds. A corona exhibits concentric colored rings centered on the light source, ranging from blue or green on the inside to red on the outside. Iridescence, on the other hand, presents a patchwork of colors, especially along cloud edges. Both phenomena are created by wavelength-dependent scattering of light by cloud particles. The size, shape, and color purity of either display depend on the cloud particle size and distribution, and on the optical thickness of the cloud (e.g., Gedzelman and Lock 2003). Generally, the colors are of a pastel nature, with low purity, because of the high content of white light combined with the scattered colors.

Coronas and iridescence have provided interesting scientific questions for multiple generations of scientists and naturalists. One of the earliest discussions in the literature readily available to us is by George Simpson, Meteorologist to the first British Antarctic Expedition led by Captain Scott (Simpson 1912). Simpson described being enveloped in fog on the coast of McMurdo Sound in Antarctica, observing circular rings of color centered on the sun as the fog dissipated in air temperatures ranging from  $-15^{\circ}$  to  $-21^{\circ}\text{F}$  ( $-26^{\circ}$  to  $-29^{\circ}\text{C}$ ). Based on the absence of halos accompanying this display, Simpson concluded that coronas are the result of diffraction by water droplets, not by ice crystals. In fact, he stated that corona observations were a tool that could determine the composition of a cloud: "If there is a corona the cloud must be composed of water, while if there is a halo it must be composed of ice" (Simpson 1912). Because supercooled water droplets provide the opportunity for coronas to exist in clouds at such cold temperatures, it is indeed a valid question to ask whether coronas and iridescence are generated by liquid or ice. Even the geometry of the corona cannot easily provide an answer to this question because a circular corona can conceivably result from diffraction by spherical water droplets or by randomly oriented needle-shaped ice crystals. In more recent years, understanding of the particle characteristics responsible for corona and iridescence formation has benefited from modern computing capability and remote sensing measurements. For example, Sassen (1991) used polarization lidar data and diffraction calculations of particle diameters from corona photographs to demonstrate that coronas can indeed be created by ice clouds, despite the earlier questioning by himself (Sassen 1979) and others (e.g., Simpson 1912). Somewhat later, Sassen et al. (1998) used ground-based polarization lidar and radar measurements, along with corona photographs and airborne cloud-particle

collectors, to confirm that individual corona displays were produced by unusually small nonspherical ice crystals of mean dimension approximately  $25\ \mu\text{m}$ , in thin, cold ( $\sim -70^{\circ}\text{C}$ ) cirrus clouds.

Most coronas are nearly circularly shaped, although oblong-shaped coronas can arise from diffraction by nonspherical pollen in the clear air (Parvianen et al. 1994; Trankle and Mielke 1994). A closely related variation is nearly circular coronas that are caused by juniper pollen in the otherwise clear air (Mims 1998). In this paper an example of a circular corona is shown, as are several examples of noncircular coronas caused by a gradient in mean cloud-particle size, not particle shape.

For a plane wave incident on a circular obstruction or aperture, the Fraunhofer (far field) diffraction pattern is a set of concentric circular rings described by a Bessel function equation referred to as the Airy function (Goodman 1996). The angular radius  $\theta$  of an  $m$ th-order corona ring can be related to the optical wavelength  $\lambda$  and cloud particle diameter  $d$  through the relationship (Goodman 1996; Shaw and Neiman 2003)

$$\sin(\theta) = \frac{m\lambda}{d}, \quad (1)$$

where  $m$  is 0, 1.635, 2.679, 3.699, 4.710, . . . , for maxima, and 1.220, 2.233, 3.238, . . . , for minima. Equation (1) shows that the rings will have shorter-wavelength blue on the inside and longer-wavelength red on the outside, and that larger corona rings will result from smaller particles. Thin clouds minimize multiple scattering, and narrow particle-size distributions avoid excessive overlap of colored rings, leading to the best visual displays. Clouds with splotchy, but locally monodisperse, distributions of small particles create patterns of iridescence influenced by outlines and contours of cloud elements. A more thorough review of basic diffraction theory as it relates to this discussion is provided in the sidebar.

In this paper, an explanation is provided describing why diffraction patterns are likely to be observed with the greatest regularity downwind of significant mountain barriers where wave clouds are generated by flow over these barriers. Photographs of prominent diffraction displays through mountain wave clouds downstream of Colorado's northern Front Range communities of Boulder and Nederland (locations shown in Fig. 1) are then shown, and mean cloud-particle diameters are inferred from the measured maxima for red and blue light in the corona photographs.

## DIFFRACTION THEORY FOR UNDERSTANDING CORONAS AND IRIDESCENCE

Coronas and iridescence are two closely related types of colorful displays in clouds. A corona exhibits concentric colored rings centered on the light source, ranging from blue or green on the inside to red on the outside. Iridescence, on the other hand, presents a patchwork of colors influenced by outlines and contours of cloud elements. Both phenomena are created by wavelength-dependent scattering of light by cloud particles. The size, shape, and color purity of either display depend on the cloud particle size and distribution, and on the optical thickness of the cloud. Generally the colors are of a pastel nature, with low purity, because of a combination of color smearing by a broad particle-size distribution, cloud optical thickness, and the high content of white light combined with the diffracted colors.

Clouds usually appear white or gray to human observers, in part because their particles are typically at least an order of magnitude larger than the wavelength of visible light (~0.38–0.68  $\mu\text{m}$  for violet through red), resulting in nearly wavelength-independent scattering (multiple scattering also plays a role). Atmospheric gas molecules, conversely, are much smaller than the wavelength of visible light and result in scattering that varies with the inverse fourth power of wavelength (Rayleigh scatter). Therefore, a sun low in the sky sends light along a long atmospheric path to illuminate a cloud near the observer with orange/red light, and the cloud acts like a nearly wavelength-independent screen to display this light. However, when a cloud is optically thin and contains a relatively narrow particle-size distribution, colored scattering effects can become visible at certain angles corresponding to rainbows, glories, and coronas. Closed-form solutions of the relevant electromagnetic scattering theory generally are limited to special cases, such as particles that have spherical (Mie scatter), cylindrical, or otherwise simple geometry or symmetry (Bohren and Huffman 1983). A much simpler approach, however, is to use scalar diffraction theory, which provides a polarization-independent (scalar) approximate solution for scattering by objects or apertures that are larger than the optical wavelength (Goodman 1996). Some of the light impinging on such an object is deviated from its prior course, or diffracted, into a new direction that depends on wavelength and object size.

The simplest form of scalar diffraction theory is obtained in the Fraunhofer approximation, valid for diffraction patterns observed at a distance much greater than  $\pi d^2 / \lambda$ , where  $d$  is the maximum transverse object dimension (i.e., particle diameter) and  $\lambda$  is the optical wavelength. At such

distances, the diffraction pattern is proportional to the spatial Fourier transform of the object. Corona and iridescence in clouds easily satisfy this condition for ground-based observers.

The irradiance ( $\text{W m}^{-2}$ ) in a Fraunhofer diffraction pattern for a uniformly illuminated circular object of diameter  $d$  is described by the Airy function,

$$I(r) = \left( \frac{\pi d^2}{4\lambda z} \right)^2 \left[ \frac{2J_1\left(\frac{\pi dr}{\lambda z}\right)}{\left(\frac{\pi dr}{\lambda z}\right)} \right]^2, \quad (\text{S1})$$

where  $r$  is the radial coordinate in the observation plane,  $\lambda$  is the optical wavelength,  $z$  is the distance from the object to the observer, and  $J_1$  is a first-order Bessel function of the first kind. The Airy pattern in Eq. (S1) is a set of concentric rings, often described in terms of their angular radius  $\theta$  (the angle by which the light is deviated upon encountering the particle). Because Fraunhofer theory is only valid for small angles, some sort of small-angle approximation is common, resulting in the Bessel function argument being written in one of the following forms:

$$\frac{\pi dr}{\lambda z} = \frac{\pi d \tan(\theta)}{\lambda} \approx \frac{\pi d \sin(\theta)}{\lambda} \approx \frac{\pi d \theta}{\lambda}. \quad (\text{S2})$$

We choose to use the  $\sin(\theta)$  version of Eq. (S2), describing the angular position of maxima and minima in the oscillating Airy pattern with

$$\sin(\theta) = \frac{m\lambda}{d}, \quad (\text{S3})$$

where  $m$  is a constant (0, 1.635, 2.679, 3.699, 4.710, . . . , for maxima and 1.220, 2.233, 3.238, . . . , for minima). Notice that Eq. (S3) shows that the rings will have shorter-wavelength blue on the inside and longer-wavelength red on the outside, and that larger corona rings will result from smaller particles. Thin clouds minimize multiple scattering, and narrow particle-size distributions avoid excessive overlap of colored rings, leading to the best visual displays. Clouds with splotchy, but

*(continued on next page)*

locally monodisperse, distributions of small particles create patterns of iridescence.

In this paper, the mean cloud-particle sizes are inferred from the measured maxima for red and blue light in corona photographs taken with lenses of known focal length. The maxima are used because it allows one to most reliably identify the wavelength appropriate for any point in the photograph. This approach differs only in minor respects from that of previous studies (Simpson 1912; Lock and Yang 1991; Sassen 1979, 1991; Sassen et al. 1998), which used a slightly simpler approximation for the angular minima in

circular diffraction patterns:  $\sin(\theta) = (n + 0.22)\lambda/d$ . This equation approximates the angular location of the  $n$ th-order minimum and has traditionally been used with a green wavelength of  $0.57 \mu\text{m}$ , which is assumed to coincide with the red maximum. However, Lock and Yang (1991) showed that Fraunhofer diffraction theory agreed better with Mie scattering calculations if a blue wavelength of  $0.49 \mu\text{m}$  was used instead of the traditional green  $0.57 \mu\text{m}$ . In the discussion section of this paper we show that blue is the more appropriate short-wavelength color for optically thin wave clouds.

Additional inferences about the wave–cloud microphysics based on analysis of these photographs are also offered. A significant result of the diffraction analysis summarized here is that coronas and iridescence in mountain wave clouds can be created by tiny quasi-spherical ice particles that may be commonly associated with this class of clouds (Shaw and Neiman 2003), whereas previous documentation of coronas produced by ice particles was limited to relatively rare observations within nonorographic cirrus clouds composed of unusually small, but nonspherical, ice crystals (e.g., Sassen 1991; Sassen et al. 1998). In our companion paper (Shaw and Neiman 2003), many of the same photographs were used to focus on the issue of colors in coronas within mountain wave clouds; in contrast, this present contribution is intended as an overview for the meteorological community and places a greater emphasis on the related mountain meteorology. Above all, publishing this paper in *BAMS* was motivated by our desire to share some of the more aesthetically beautiful aspects of the field of meteorology with our colleagues.

**MOUNTAIN WAVE CLOUDS: MACROPHYSICAL AND MICROPHYSICAL CHARACTERISTICS.** Based on a long and productive history of observational, numerical, and analytic research in mountain meteorology, it is commonly known that mountainous terrain can excite significant atmospheric gravity–wave (i.e., mountain–wave) activity when stably stratified ambient flow impinges upon these topographic barriers (e.g., Queney 1948; Lilly and Zipser 1972; Klemp and Lilly 1975; Smith 1979; Durran 1986; Clark et al. 1994; Carney et al. 1996; Ralph et al. 1997; Whiteman 2000; Doyle and Shapiro 2000; among many others). These waves typically take on one of two forms: vertically

propagating mountain waves that usually have their largest amplitude well above the mountain peak and vertically trapped lee waves that are typically confined to the downwind side of the peak and at somewhat lower levels (e.g., Figs. 2a,b). The type of wave that forms is dependent on the shape and height of the mountain barrier, as well as on the static stability and wind characteristics upwind of the barrier. It is not uncommon for both wave types to exist simultaneously as a hybrid mode. The amplitude of the mountain–wave activity tends to be largest when tall, wide, and quasi-two-dimensional mountain ranges that are steepest on their leeward flank protrude into strong ambient flow directed roughly perpendicular to the two-dimensional barrier. Therefore, the western United States is a prime region for mountain–wave generation, because many of its mountain ranges are linearly oriented north–south and intercept the prevailing deep-tropospheric westerly flow during the cooler months. The Front Range communities of northeastern Colorado, including Boulder, are especially prone to mountain–wave activity because the mountain barrier (i.e., the Continental Divide) that excites the waves is not only oriented north–south, but is tall, wide, and quite steep on its eastern face (Fig. 1).

Mountain waves can cause damaging downslope windstorms and pose a significant risk to aviation. But these waves also provide aesthetic appeal by generating beautiful and odd-looking standing lenticular wave clouds in the wave crests when sufficient moisture is present in thin laminar layers (e.g., Smith 1979; Durran 1986; Houze 1993; Carney et al. 1996; Whiteman 2000). Lenticular clouds are known to accompany both vertically propagating and vertically trapped mountain waves (Figs. 2a,b). A photographic example of each class of wave cloud is shown in Figs. 2c and 2d. These clouds are often thin and lens-

shaped and are sometimes stacked in multiple layers, thus reflecting the filamented moisture structure commonly found in stably stratified flow upstream of the topographic barrier exciting the wave clouds. The small thickness of these laminar moisture layers, the large ratio of the horizontal-to-vertical air motion within these clouds, and the fact that there is a limited amount of time for cloud particles to fall as they are quickly transported through the wave cloud all contribute to the thin character of these lenses. Since individual lenticular lenses are characteristically thin, they tend to be translucent, thus readily allowing sunlight or moonlight to penetrate them. Because of Boulder's location relative to the Continental Divide (Fig. 1), lenticular wave clouds are common there.

Lenticular wave clouds are composed of particles whose sizes ( $\leq 25 \mu\text{m}$ ; Heymsfield and Miloshevich 1993, 1995) are much smaller than those of nonorographic ice-crystal cirrus clouds ( $> 100 \mu\text{m}$ ; e.g., Heymsfield and Platt 1984; Platt et al. 1989; Sassen et al. 1989), except for very cold cirrus clouds ( $< -60^\circ\text{C}$ ) whose ice crystals can be comparable in size (e.g., Heymsfield 1986; Platt et al. 1989; Sassen 1991; Sassen et al. 1998). In contrast, most nonorographic liquid-phase clouds contain particles that are similar in size to those of the wave clouds (e.g., Pruppacher and Klett 1980; Heymsfield 1993; Heymsfield and Miloshevich 1993, 1995). Because wave clouds can be characterized by quasi-steady-state air motions and microphysical properties (e.g., Heymsfield and Miloshevich 1993, 1995), the wave-cloud particles exhibit a much narrower range of sizes than the nonorographic cloud particle (Pruppacher and Klett 1980; Heymsfield and Miloshevich 1995; Gerber et al. 1998; Jensen et al. 1998). The nearly uniform size of orographic cloud particles is caused by rapid ( $< 1\text{--}2 \text{ min}$ ) condensation arising from fierce competition of available moisture due to strong wave-induced upward motion ( $> 2\text{--}8 \text{ m s}^{-1}$ ; Heymsfield and Miloshevich 1993, 1995).

Wave clouds can, and usually do, consist of particles in a supercooled state in temperatures as low as  $-36^\circ\text{C}$  (e.g., Heymsfield and Miloshevich 1993), though in conditions that approach  $-40^\circ\text{C}$ , water can exist naturally only in solid form (Pruppacher and Klett 1980). Microphysical studies of wave clouds have shown that droplets freeze spontaneously at the homogeneous nucleation point, typically between about  $-36^\circ$  and  $-38^\circ\text{C}$  (e.g., Sassen and Dodd 1988; Heymsfield and Miloshevich 1993, 1995), and that these frozen particles retain the spherelike shape of their liquid-phase counterparts (Gerber et al. 1998; A. J. Heymsfield 2001, personal communication;

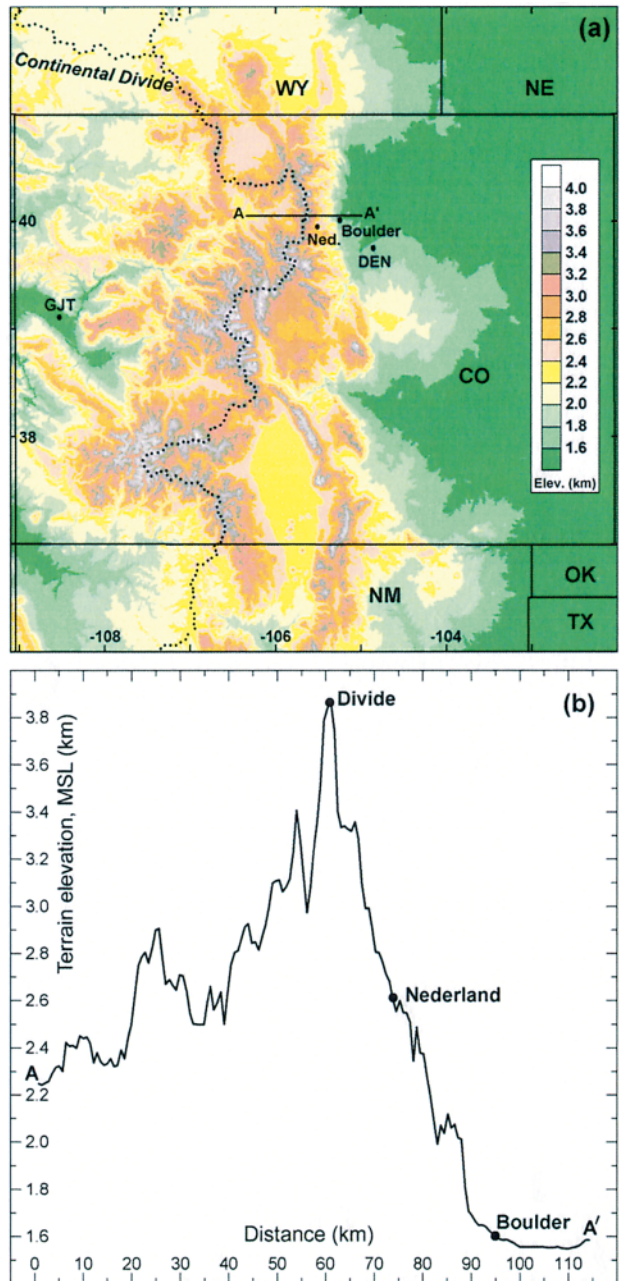


**FIG. 1.** (a) Terrain base map of Colorado and vicinity showing the sites where twice-daily operational rawinsondes were launched (DEN: Denver; GJT: Grand Junction). The black dotted line marks the Continental Divide. Latitude and longitude labels are on the left and bottom, respectively. Line AA' is the projection for the cross section of terrain elevation (km) above mean sea level in (b). All photos presented in this paper were taken in Boulder or Nederland [i.e., "Ned." in (a)].

Shaw and Neiman 2003). In general, the frozen spheres are larger in size than the liquid droplets; that is, the former can approach  $25 \mu\text{m}$  in diameter, whereas the latter are typically restricted to sizes less than  $\sim 15 \mu\text{m}$  (e.g., Heymsfield and Miloshevich 1993,

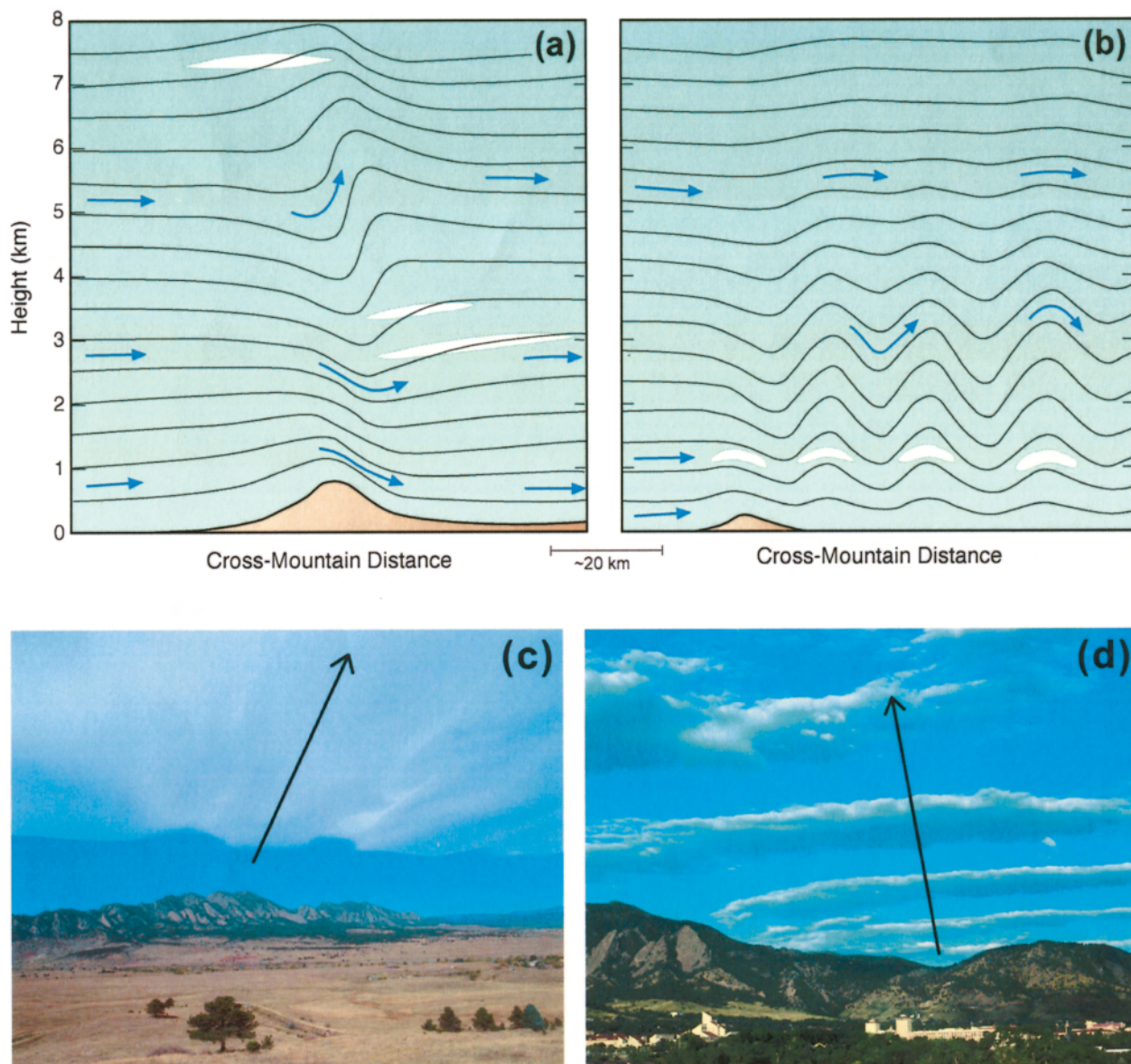


**FIG. 2.** Schematic of lenticular clouds (white lenses) resulting from (a) vertically propagating mountain waves and (b) vertically trapped lee waves; and photographs of wave clouds near Boulder, Colorado, resulting from (c) vertically propagating mountain waves and (d) vertically trapped lee waves. The solid contours in (a) and (b) portray streamlines in the plane of the projection, and the blue arrows show the direction of flow. Panels (a) and (b) are adapted from Whiteman (2000). The black arrows in (c) and (d) portray the approximate direction of flow at cloud level. Note that the wave clouds in (d) do not exhibit filamented lenticular structure; this photo is shown primarily to illustrate the family of parallel cloud bands that can occur with trapped lee waves.

1995). The small mean size, narrow range of sizes, and pseudo-spherical shape of cloud particles within lenticular clouds, together with the translucent character of these clouds, make lenticulars an ideal type of cloud for producing well-defined and colorful diffraction patterns of coronas and iridescence (e.g., see Fig. 3 illustrating iridescent lenticular wave clouds).

**EXAMPLES OF CORONAS AND IRIDESCENCE.** In this section, we showcase eight examples

of solar diffraction/scattering patterns within lenticular wave clouds observed east of Colorado's Continental Divide above Boulder and Nederland (see Fig. 1 for locations). These patterns ranged from a fully circular corona to patchwork iridescence. The dates and meteorological characteristics of these eight cases are summarized in Table 1. Twice-daily operational rawinsonde launches from Denver and Grand Junction in Colorado (Fig. 1) provided measurements of the background meteorological conditions. All eight cases

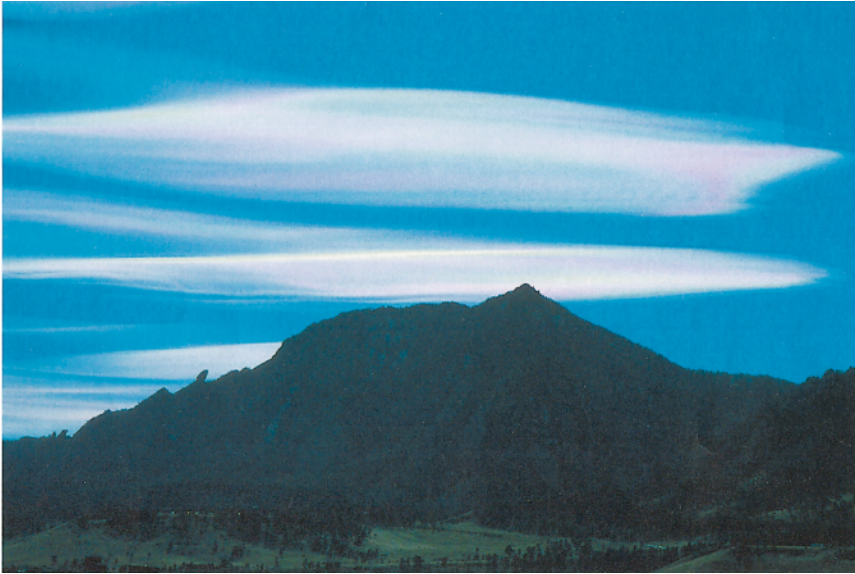


**FIG. 3. Photograph of iridescent standing lenticular wave clouds above Boulder, Colorado, on 8 Nov 1995. This cropped photo was taken with a 70–210-mm focal length lens; the exact focal length is unknown.**

quite likely contributed to the generation of mountain-wave activity and the wave clouds. In an attempt to deduce the approximate heights, temperature characteristics, and microphysical phase of these wave clouds, the heights and temperature ranges of prominent moist layers (defined by a dewpoint depression of  $< \sim 5^{\circ}\text{C}$ ) at Denver and Grand Junction are also shown in Table 1. It is reasonable to assume, though impossible to confirm,<sup>1</sup> that the wave clouds that produced the diffraction patterns resided within

exhibited west to northwest flow near mountain top in the layer between 700 and 500 mb, or about 3.0–5.5 km above mean sea level (MSL). The associated cross-mountain or west-to-east component of this layer-mean flow was significant ( $7.1\text{--}17.4\text{ m s}^{-1}$ ) and

<sup>1</sup> Because the wave clouds that produced the diffraction patterns were thin and localized, infrared satellite imagery could not provide meaningful information about cloud-top temperature (hence cloud-top height) for most of the cases presented in this paper.

**TABLE 1. Mean wind, moisture, and temperature characteristics from the relevant Denver and Grand Junction rawinsonde soundings for the diffraction displays shown in the photographs. Inferred cloud particle sizes are also shown for each display (where applicable).**

Fig. no.	Date	700–500-mb mean wind information			Moist layers* (mb)	Temperature range of moist layers ( $^{\circ}\text{C}$ )	Inferred cloud particle size ( $\mu\text{m}$ )
		Direction ( $^{\circ}$ )	Speed ( $\text{m s}^{-1}$ )	Cross-mountain ( $\text{m s}^{-1}$ )			
4	5 Nov 1989	280	17.7	17.4	650–547; 511–386; 450–320	5.1–14.4; 16.0–29.7; 22.0–39.9	20.4
5	29 Jan 1987	301	13.6	11.7	565–429; 400–331	15.5–28.2; 31.9–39.9	19.5–24.3
6	31 May 1987	262	7.2	7.1	638–562; 550–500; 420–363	0.1–8.2; 6.7–9.1; 18.3–25.7	7.6–16.6
7	31 Oct 1989	283	14.0	13.6	559–493; 474–443; 457–341	16.9–24.5; 23.2–26.1; 24.1–39.8	14.4–18.1
8	15 Jan 1996	271	14.4	14.4	552–529; 387–100	12.0–13.6; 31.1–65.2	—
9	3 Jan 1987	285	12.6	12.2	584–312	10.1–40.0	—
10a, 3	8 Nov 1995	294	15.0	13.7	315–100	38.9–70.7	—
10b	25 Dec 1998	310	17.3	13.3	579; 440–420; 300–250	15.9; 30.7–33.5; 52.5–58.3	—

\*A moist layer is defined here by a local minimum ( $< \sim 5^{\circ}\text{C}$ ) of dewpoint depression in a rawinsonde profile.

these moist layers, all of which were colder than the melting level (i.e.,  $< 0^{\circ}\text{C}$ ). This moisture information can only be used qualitatively, since spatial variations in moisture are often quite significant. It should be emphasized that polarization lidar and in situ probes provide the only accurate measurements of the microphysical and thermodynamic attributes within clouds. Unfortunately, we did not have these instruments at our disposal during the corona and iridescence displays highlighted in this article.

**Coronas.** When sunlight or moonlight passes through translucent clouds composed of particles that are sufficiently small and uniform in size, corona rings will result. The angular radius of a given order of colored rings is inversely proportional to the size of the dominant cloud particles producing the corona. Analysis of corona photographs provides a reasonably accurate passive remote sensing method to determine the dominant cloud particle size, assuming that the focal length of the camera lens is known. In this section, we deduce the dominant cloud particle sizes and their spatial distributions within wave clouds by analyzing photographs of four coronal displays. Mean wavelengths of  $0.63$  and  $0.48\ \mu\text{m}$  are used to determine the angular radii of the red and blue coronal rings, respectively, in this analysis. A common attribute linking these examples, and many other corona displays we have observed in mountain wave clouds, is the vividness of the blue color, often at the expense of green. This issue is explored in more detail in Shaw and Neiman (2003) and in the discussion section of this paper.

**CIRCULAR CORONA.** The corona in Fig. 4 was circular and exhibited unusually rich color. Hence, the population of wave-cloud particles that produced this striking display contained a very narrow range of sizes that were evenly distributed throughout this portion of the cloud. The angular radii of the first-order red ring and second-order blue and red rings were measured at four locations in this photo, and the average radii are shown to the right of the sun. From Eq. (1), these values correspond to a mean cloud particle diameter of  $20.4\ \mu\text{m}$  ( $\pm 0.5\ \mu\text{m}$ ), which is comparable to in situ aircraft observations of frozen particle sizes within wave clouds (e.g., Heymsfield and Miloshevich 1993, 1995).

Based on the meteorological data summarized in Table 1, this wave cloud could have resided in one of three layers that extended collectively through a deep layer of the troposphere from 650 to 320 mb (i.e., from about  $-5^{\circ}$  to  $-40^{\circ}\text{C}$ ). However, the contrail in

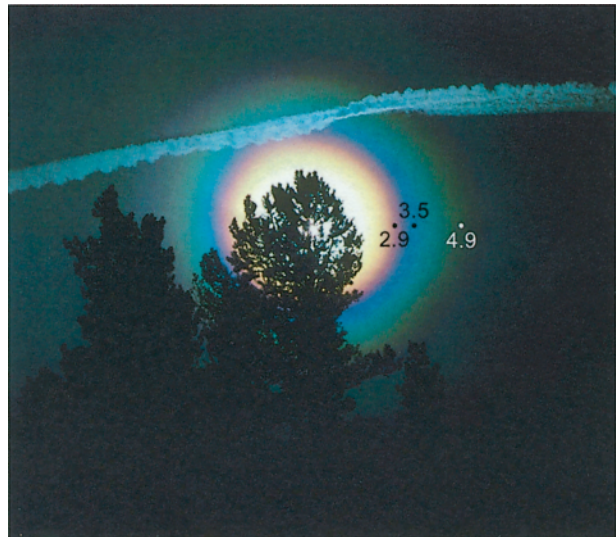


**FIG. 4.** Photograph of a circular corona above Nederland, Colorado, on 5 Nov 1989. The first-order red ring and second-order blue and red rings are marked to the right of the sun, and their radii are labeled in degrees. This cropped photo was taken with a 70-mm focal length lens.

this photo can be used to constrain the estimate of the vertical position and temperature of the cloud. Because contrails form at temperatures below about  $-43^{\circ}\text{C}$  (Appleman 1953),<sup>2</sup> it is deduced from the nearby rawinsonde soundings that this contrail could not have resided at lower than  $\sim 9$  km MSL, or about 6.4 km above ground. Furthermore, the original photograph reveals that the contrail cast a sharp but very narrow ( $< 0.3^{\circ}$  of arc) shadow on the wave cloud, though this shadow may be difficult to see in the single-column reproduction (Fig. 4). In this photo, the shadow is located directly above the contrail and only to the left of the sun, thus suggesting that the contrail was slightly above the wave cloud in the left portion of the photo and within the cloud on the right side. Knowing that the maximum possible sun angle for the date of the photo is  $\sim 33.5^{\circ}$  and then performing the appropriate simple geometry, the contrail could not have extended more than  $\sim 25$  m above the cloud. And given that the wave cloud was quite thin (i.e., note the sharp detail of the contrail through the wave cloud), the wave cloud effectively resided at the level of the contrail—that is, at a temperature  $\leq -43^{\circ}\text{C}$  or slightly above the uppermost moist layer measured by the soundings. At these

<sup>2</sup> This temperature corresponds to a cruising altitude of 300 mb. For higher cruising altitudes, the critical temperature at which contrails can form decreases.

very cold temperatures, water can exist naturally only in solid form (Pruppacher and Klett 1980); hence the wave-cloud particles most likely were composed of ice. The relatively large wave cloud particle diameter of  $20.4 \mu\text{m}$  inferred from the angular radii of the coronal rings further supports this conclusion. Reports of ice-crystal coronas have also been described in the literature within nonwavelike cirrus cloud sheets (e.g., Sassen 1991; Sassen et al. 1998), though these displays are relatively uncommon since the ice crystals in this species of cloud are nonspherical and often too large (i.e.,  $> \sim 100 \mu\text{m}$ ; Heymsfield and Platt 1984; Platt et al. 1989; Sassen et al. 1989) to produce a visible corona.

**NONCIRCULAR CORONAS.** Wave cloud particles can be sufficiently uniform in size to produce noticeable diffraction rings, but they may vary enough in size across the cloud such that these rings are noncircular. This subsection highlights four variants of noncircular coronas. Where possible, Eq. (1) is used to determine the particle diameter corresponding to the angular “radius” at different points within the noncircular diffraction pattern.

**OBLONG.** The diffraction rings of the oblong-shaped corona in Fig. 5 became gradually smaller from the top of the photo to the bottom. The mean cloud particle diameters that were deduced from the angular radii of these rings ranged from  $19.5 \mu\text{m}$  at the top of the corona to  $24.3 \mu\text{m}$  at the bottom. These relatively

large diameters suggest that the wave clouds were composed of ice particles. Temperature measurements summarized in Table 1 do not refute this interpretation, since the upper portion of the higher moist layer was colder than the homogeneous nucleation point. It is likely that the change of angular radii reflected the growth of ice particles in the upward-motion portion of the wave cloud, especially given that a small component of the upper-tropospheric flow was directed from the top of the corona (near the upwind edge of the cloud) to the bottom. This oblong corona was generated by a spatial variation in cloud particle size distribution across the corona, whereas previous studies describe oblong coronas resulting from diffraction by oblong-shaped pollen (Parviainen et al. 1994; Trankle and Mielke 1994).

**ASYMPTOTIC.** The rather uniquely shaped high-order corona shown in Fig. 6 was observed at the upwind edge of a wave cloud and represents an extreme example of noncircular coronas. The angular radii of the first- through fourth-order red rings above the sun correspond to cloud particle diameters of  $12.3$ ,  $14.5$ ,  $15.8$ , and  $16.6 \mu\text{m}$ , respectively, while the mean radius of the first-order red ring near the edge of the cloud was produced by an average particle diameter of  $7.6 \mu\text{m}$ . The relatively small size of these particles, and the fact that the prominent moist layers remained well below the homogeneous nucleation point (Table 1), indicate that the wave cloud was composed of water droplets. Because the upwind edge of the

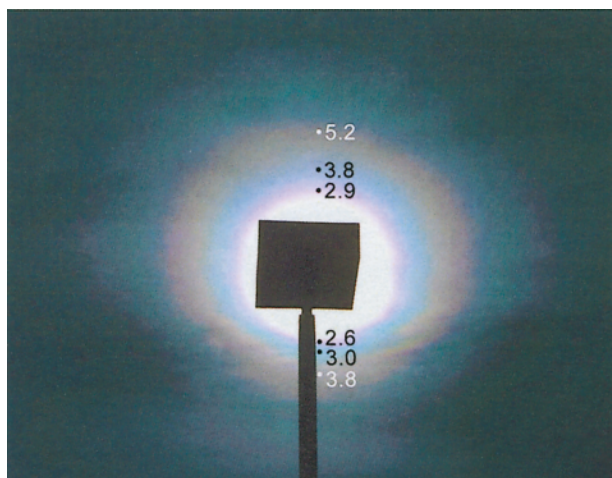


**FIG. 5.** Photograph of an oblong corona above Boulder, Colorado, on 29 Jan 1987. The first-order red ring and second-order blue and red rings are marked below and above the sun, and their radii are labeled in degrees. This cropped photo was taken with a 70-mm focal length lens.

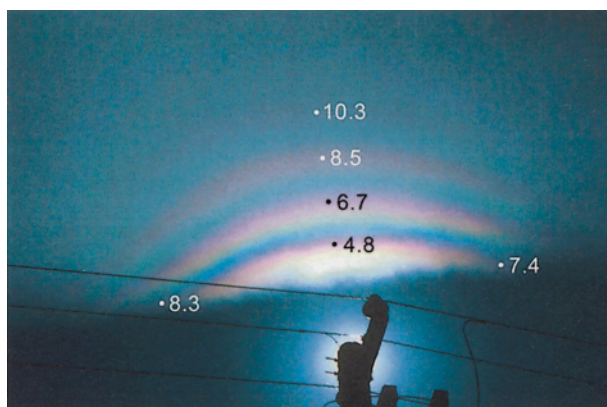


**FIG. 6.** Photograph of an asymptotic corona at the upwind edge of a wave cloud above Nederland, Colorado, on 31 May 1987. The first-order red ring is marked above and to the sides of the sun, and the second-through fourth-order red rings are marked above the sun; their angular radii are labeled in degrees. This cropped photo was taken with a 70-mm focal length lens.

cloud is where the limit of the droplet size goes to zero, the angular radii of the diffraction rings here became quite large. Hence, we refer to this particular diffraction display as an asymptotic corona.

The fortuitous location and unique shape of these diffraction rings, in tandem with knowledge from rawinsonde observations that midtropospheric flow of  $\sim 10 \text{ m s}^{-1}$  was directed nearly perpendicular to the cloud edge from bottom to top, provide useful information about the distribution of cloud particles and their mean growth rate at the upwind edge or updraft region of this wave cloud. The decrease in radii of the diffraction rings (i.e., the increase in droplet size) from the upstream edge of the cloud to its interior clearly documented the growth of cloud droplets. Assuming steady horizontal flow of  $10 \text{ m s}^{-1}$  through the wave cloud, the most rapid growth rate occurred at the leading edge of the cloud where droplets initially formed and reached a mean diameter of  $7.6 \mu\text{m}$  in less than  $\sim 5 \text{ s}$ . Thereafter, the droplets increased in size much more slowly to  $16.6 \mu\text{m}$  in either  $\sim 34$  or  $\sim 70 \text{ s}$ , depending on whether the cloud was assumed to reside in the lower or upper moist layer ( $\sim 638$  to  $500 \text{ mb}$  or  $420$  to  $363 \text{ mb}$ ) summarized in Table 1. The initial rapid cloud-droplet growth and subsequent slow growth within the updraft region of the wave cloud's upwind edge is fully consistent with in situ aircraft observations of droplet growth in the same region of other liquid-phase wave clouds (Heymsfield and Miloshevich 1993).

**STEPWISE.** The coronal display in Fig. 7 exhibited an abrupt stepwise change in the angular radii of its rings above the sun. The relatively circular rings that comprised the lower two-thirds of this corona correspond to a mean particle diameter of  $18.1 \mu\text{m}$ , a value that is representative of frozen wave-cloud particle sizes. In contrast, the partial rings possessing larger angular radii above the sun were created by a much smaller mean particle diameter of  $14.4 \mu\text{m}$  that is more characteristic of wave-cloud water droplets. Multiple moist layers were observed during this event (Table 1), the highest of which extended above the homogeneous nucleation point. Heymsfield and Miloshevich (1993) presented in situ observations of a rapid change in phase of wave-cloud particles, from supercooled liquid to ice, and a corresponding jump in particle size, associated with homogeneous nucleation. Therefore, it is plausible that the discrete change in the angular radii of the coronal rings in this photograph marks the location of a phase change from supercooled liquid (larger rings; top) to ice (smaller rings; bottom), although other factors, such as a com-

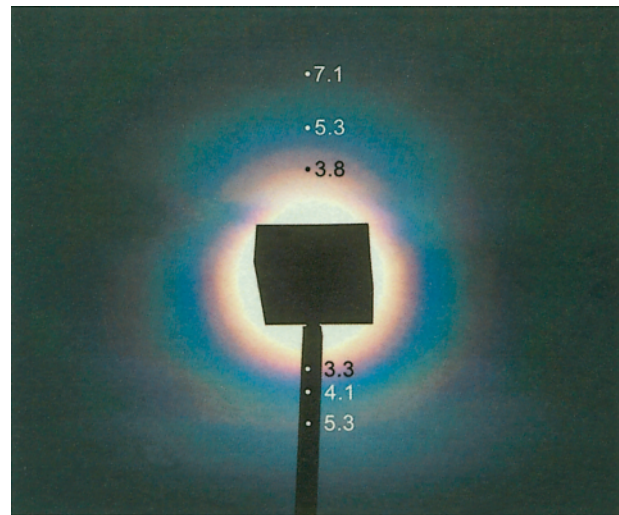


**FIG. 7. Photograph of a stepwise corona above Boulder, Colorado, on 31 Oct 1989. The first-order red ring and second-order blue and red rings are marked below and above the sun, and their radii are labeled in degrees. This cropped photo was taken with a 70-mm focal length lens.**

plicated wave pattern, may have contributed to or resulted in this discrete change.

**RAGGED.** The corona in Fig. 8 was photographed using a zoom lens. Because the precise focal length was unknown in this case, we were unable to accurately determine the mean cloud-particle size(s) that produced this corona. Nevertheless, the photo clearly highlights a ragged or rough-edged character to the diffraction rings. This distinctive trait indicates that the cloud particles were sufficiently uniform in size to produce coherent rings, but that these particles also exhibited enough variability in size across the cloud to create undulations within these rings.

This case is unique among those presented in this section because it was characterized by a superposition of high-level wave clouds east of the Continental Divide and synoptic-scale cirrus streaming overhead from southern California (cloud-top temperatures  $< -50^\circ\text{C}$ , satellite imagery not shown). The soundings clearly documented this upper-level moisture up to  $100 \text{ mb}$  or  $\sim -65^\circ\text{C}$ , as well as a very thin moist layer in the middle troposphere (Table 1). At the time this photo was taken, however, midtropospheric wave clouds were not evident in the immediate vicinity. Therefore, it is quite likely that both the wave clouds and cirrus in the area were composed of ice particles. Because the cirrus was quite cold, its ice crystals were probably small enough to produce the corona (e.g., Platt et al. 1989; Sassen 1991; Sassen et al. 1998) in

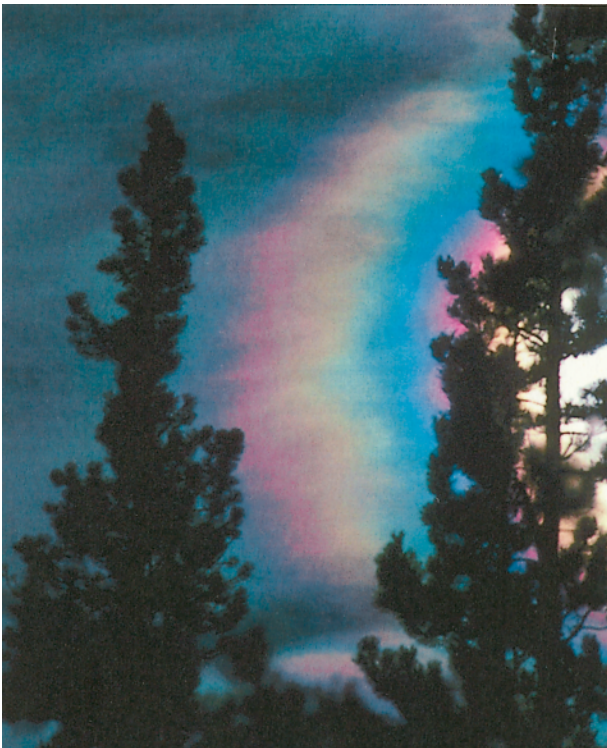


**FIG. 8.** Photograph of a ragged corona above Nederland, Colorado, on 15 Jan 1996. This cropped photo was taken with a 70–210-mm focal length lens; the exact focal length is unknown.

tandem with the upper-level wave clouds. Based on the microphysical characteristics of nonorographic cirrus clouds outlined in section 2, the cirrus ice particles in this case exhibited a comparatively large range of sizes (relative to wave-cloud ice particles) and were nonspherical and randomly oriented. Therefore, the cirrus ice crystals quite likely contributed to the ragged appearance of the coronal rings.

**AUREOLE.** Figure 9 shows a relatively diffuse and ruddy-colored corona surrounding the solar disk. This type of corona, commonly referred to as aureole, is caused either by relatively large cloud-particle sizes that constrict the diffraction rings close to the sun or moon, or by a broad spectrum of particle sizes randomly distributed throughout an optically thick cloud that cause the colored rings to overlap. Given that the photo shows a faint sprinkling of colors quite far (i.e., as far as  $\sim 15^\circ$ ) from the sun, small cloud particles were present. Therefore, this aureole resulted from the latter of the two scenarios described above. Three-dimensional wave structure was clearly evident in the cloud field, hence a large variation in cloud-particle sizes should be expected within this complex region of superimposed wave-induced upward and down-

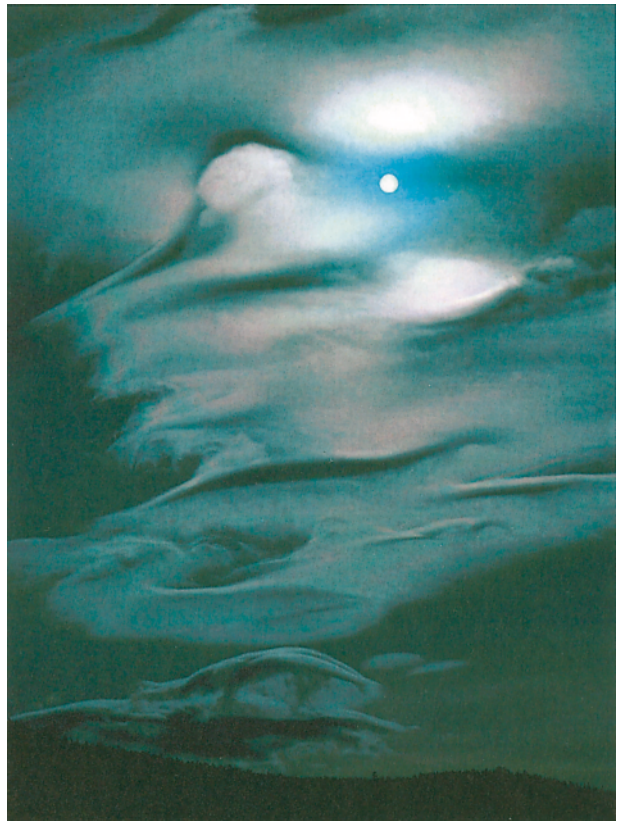


**FIG. 9.** Photograph of a corona aureole above Nederland, Colorado, on 3 Jan 1987. This cropped photo was taken with a 70-mm focal length lens.

ward motion. The sounding data (Table 1) indicated a deep layer of moisture between  $-10^\circ$  and  $-40^\circ\text{C}$ . The wave clouds' hard-edged, filamented appearance and rapid finescale motion at the time of the display suggest that the aureole was most likely caused by cloud droplets.

**Iridescence.** When sunlight or moonlight passes through a translucent cloud containing clusters of uniformly sized small particles, and each cluster is characterized by a unique mean particle size, a patchwork of colors known as iridescence can be produced relatively far from the light source. Iridescence may also occur via anomalous diffraction arising from interference effects associated with sunlight or moonlight passing through a cloud composed of very small particle sizes, thus resulting in irregular color patterns quite far from the light source (i.e., Lock and Yang 1991). Two iridescence displays are shown in Figs. 10a and 10b, and they were distinguished by smooth and mottled cloud textures, respectively. During the first display (i.e., Fig. 10a), a photo was also taken of iridescent wave clouds in their entirety (Fig. 3). Based on rawinsonde observations of this

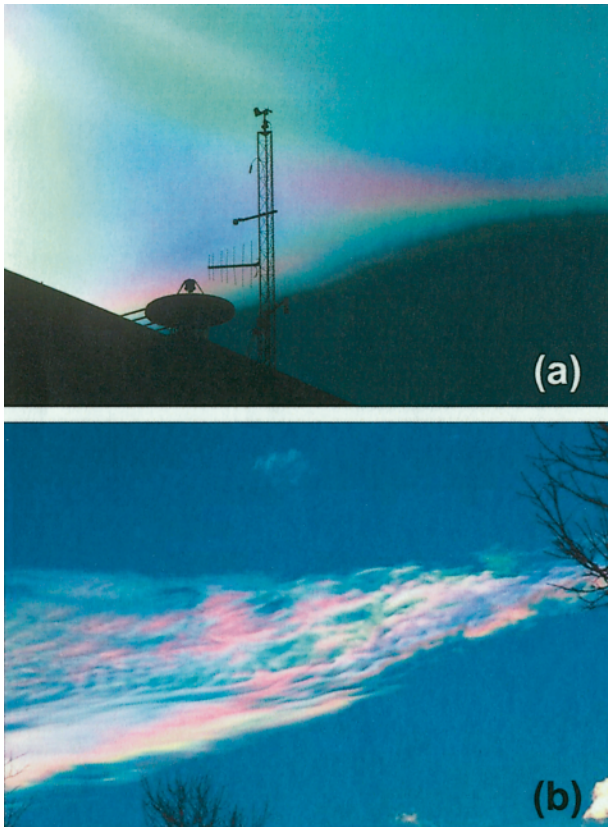


**FIG. 10. Photographs of iridescence above Boulder, Colorado, on (a) 8 Nov 1995 and (b) 25 Dec 1998. These cropped photos were taken with 70–210 and 28–200-mm focal length lenses, respectively. The exact focal length in (a) is unknown, and the focal length in (b) is ~120 mm.**

display (Table 1), moist conditions existed only at high levels where the temperature was colder than the homogeneous nucleation point. These rawinsonde observations are supported by infrared satellite imagery (not shown), showing a localized north–south-oriented wave–cloud band east of the Continental Divide over Boulder with cloud-top temperatures of  $-52^{\circ}$  to  $-58^{\circ}\text{C}$ . Hence, the iridescence in Figs. 10a and 3 was very likely produced by quasi-spherical ice particles. Rawinsonde measurements relevant to the latter display (Table 1) reveal two moist layers that were warmer than the homogeneous nucleation point and one layer that was colder. It was the impression of the authors during this display that the iridescent cloud was situated no higher than the middle troposphere—that is, in a layer where supercooled droplets would have existed. In all three iridescence photos (Figs. 3, 10a, and 10b), iridescent colors were observed at least  $10^{\circ}$ – $15^{\circ}$  from the sun, indicating that the cloud particles producing these displays were quite small, that is, the result of large-

angle (possibly high-order) diffraction. The coronal rings showcased earlier in this paper subtended smaller angles relative to the sun; hence, those particle sizes were larger.

**DISCUSSION AND FUTURE WORK.** All optical displays of coronas and iridescence presented in this paper were created by the diffraction of sunlight through lenticular wave clouds east of the Continental Divide in northeastern Colorado. Based on the ambient meteorological conditions for each display, many of these wave clouds were quite likely composed of quasi-spherical ice particles. These results suggest that diffraction displays generated by ice-phase wave clouds are common, especially during the colder months. This is in contrast to the relative rarity of diffraction displays produced by unusually small, but nonspherical, ice crystals in nonorographic cirrus clouds. The cloud particle diameters ( $7.6$  to  $24.3\ \mu\text{m}$ ) inferred from our corona photographs agree well with the theoretical particle-size range suggested by Lock and Yang (1991), based on their Mie scattering analysis of narrow and spatially uniform cloud particle-size distributions.

Future observations, combined with numerical modeling, should provide much more insight into the cloud microphysics accompanying corona and iridescence displays in mountain wave clouds, and into the perceived optical nature of these displays. In particular, we have wondered if there is a connection between the cloud particle-size distribution, or perhaps the type of cloud particle involved, and the perceived short-wavelength dominant color (green versus blue). Our observations of coronas in mountain wave clouds favor blue over green, but reports in the literature and our observations in other cloud types favor green (Shaw and Neiman 2003).

The powerful flexibility of numerical modeling provides a compelling argument that the vivid blue seen in mountain wave-cloud coronas results from the characteristically small and uniformly sized cloud particles within optically thin cloud lenses. Figure 11 shows a series of corona simulations, graciously provided by S. Gedzelman (2003, personal communication), which were obtained in a method similar to that employed by several authors of recent publications (Tränkle and Mielke 1994; Lock and Yang 1991; Laven 2003; Gedzelman and Lock 2003). The left-most panel in Fig. 11 is a circular corona calculated with Mie scattering for a narrow particle-size distribution and a thin layer of condensate typical of mountain wave clouds, using a mean particle diameter of  $16\ \mu\text{m}$  and an optical thickness of 0.1. The simulation

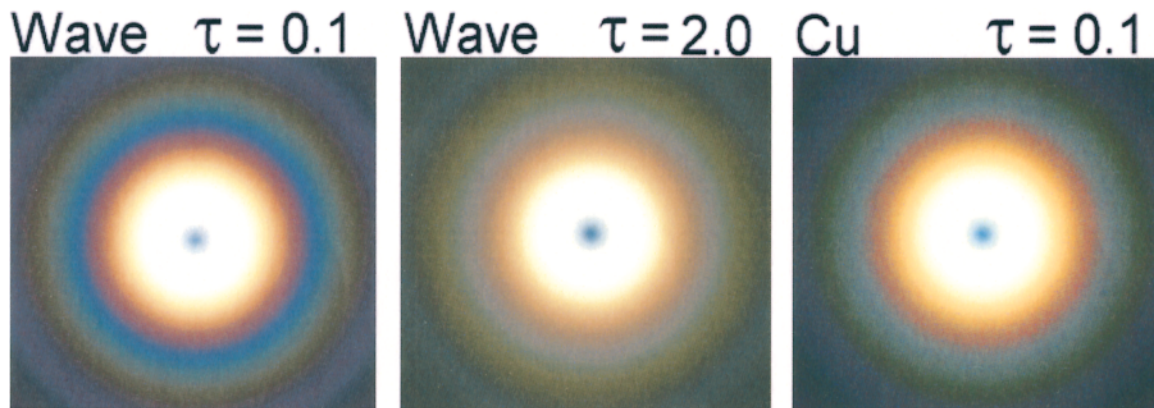


**FIG. 11.** Color-intensity simulations of (left) an optical thin wave cloud, (center) an optically thick wave cloud, and (right) an optically thin cumulus cloud, highlighting the effects of cloud optical thickness ( $\tau$ ) and droplet size distribution on the appearance of a corona (adapted from Gedzelman and Lock 2003). The wave cloud simulations utilized a vertically monodisperse droplet size distribution, and the cumulus simulation implemented a broad droplet size distribution. A maximum droplet diameter of  $16 \mu\text{m}$  was assumed.

shows remarkable similarity to the circular corona photograph in Fig. 4, including the dominant blue ring, which effectively disappears when either the optical thickness is increased to 2.0 (center panel) or the particle-size distribution is broadened to that typical of cumulus (right panel). This also illustrates the need for a more complete scattering model to investigate this sort of detail, instead of the simpler diffraction analysis.

In the future, we envision taking ground-based polarization lidar observations within mountain wave clouds to remotely ascertain microphysical attributes of these clouds during corona and iridescence displays, similar to what was done in diffraction-producing nonorographic cirrus clouds by Sassen (1991) and Sassen et al. (1998). In closing, our principal underlying hope is that this article promotes further appreciation of the beautiful and varied diffraction phenomena that carry rich information about our environment.

**ACKNOWLEDGMENTS.** We gratefully acknowledge Andy Heymsfield (National Center for Atmospheric Research) for providing microphotographs of wave cloud particles and for insightful discussions and comments about wave cloud microphysics, Ken Sassen (University of Alaska-Fairbanks) and Stan Gedzelman (City University of New York) for engaging us in stimulating discussions of coronas and iridescence and for providing thoughtful comments, Jim Churnside (NOAA/Environmental Technology Laboratory) for providing valuable feedback on the manuscript, David Whiteman (Pacific Northwest National Laboratory) for graciously allowing us to reproduce his mountain wave conceptualizations, and Allen White

(NOAA/Environmental Technology Laboratory) for generating the terrain base map information used in Fig. 1. In addition, we gratefully acknowledge Stan Gedzelman for allowing us to publish his numerical sensitivity simulations of coronas (Fig. 11).

## REFERENCES

- Appleman, J., 1953: The formation of exhaust condensation trails by jet aircraft. *Bull. Amer. Meteor. Soc.*, **34**, 14–20.
- Bohren, C. F., and D. R. Huffman, 1983: *Absorption and Scattering of Light by Small Particles*. Wiley, 530 pp.
- Carney, T. Q., A. J. Bedard Jr., J. M. Brown, J. McGinley, T. Lindholm, and M. J. Kraus, 1996: *Hazardous Mountain Winds and Their Visual Indicators*. NOAA Handbook, Environmental Research Laboratories, Boulder, Colorado, 80 pp.
- Clark, T. L., W. D. Hall, and R. M. Banta, 1994: Two- and three-dimensional simulations of the 9 January 1989 severe Boulder windstorm: Comparison with observations. *J. Atmos. Sci.*, **51**, 2317–2343.
- Doyle, J. D., and M. A. Shapiro, 2000: A multi-scale simulation of an extreme downslope windstorm over complex topography. *Meteor. Atmos. Phys.*, **74**, 83–101.
- Durrán, D. R., 1986: Mountain waves. *Mesoscale Meteorology and Forecasting*, P. S. Ray, Ed., Amer. Meteor. Soc., 472–492.
- Gedzelman, S. D., and J. A. Lock, 2003: Simulating coronas in color. *Appl. Opt.*, **42**, 497–504.
- Gerber, H., C. H. Twohy, B. Gandrud, A. J. Heymsfield, G. M. McFarquhar, P. J. DeMott, and D. C. Rogers, 1998: Measurements of wave-cloud microphysical

- properties with two new aircraft probes. *Geophys. Res. Lett.*, **25**, 1117–1120.
- Goodman, J. W., 1996: *Introduction to Fourier Optics*. McGraw-Hill, 441 pp.
- Greenler, R., 1980: *Rainbows, Halos, and Glories*. Cambridge University Press, 195 pp.
- Heymsfield, A. J., 1986: Ice particles observed in a cirriform cloud at  $-83^{\circ}\text{C}$  and implications for polar stratospheric clouds. *J. Atmos. Sci.*, **43**, 851–855.
- , 1993: Microphysical structures of stratiform and cirrus clouds. *Aerosol–Cloud–Climate Interactions*, P. V. Hobbs, Ed., Academic Press, 97–121.
- , and C. M. R. Platt, 1984: Parameterization of the particle size spectrum of ice clouds in terms of the ambient temperature and ice water content. *J. Atmos. Sci.*, **41**, 846–855.
- , and L. M. Miloshevich, 1993: Homogeneous nucleation and supercooled liquid water in orographic wave clouds. *J. Atmos. Sci.*, **50**, 2335–2353.
- , and —, 1995: Relative humidity and temperature influences on cirrus formation and evolution: Observations from wave clouds and FIRE II. *J. Atmos. Sci.*, **52**, 4302–4326.
- Houze, R. A., Jr., 1993: *Cloud Dynamics*. Academic Press, 573 pp.
- Jensen, E. J., and Coauthors, 1998: Ice nucleation processes in upper tropospheric wave clouds observed during SUCCESS. *Geophys. Res. Lett.*, **25**, 1363–1366.
- Klemp, J. B., and D. K. Lilly, 1975: The dynamics of wave-induced downslope winds. *J. Atmos. Sci.*, **32**, 320–339.
- Laven, P., 2003: Simulation of rainbows, coronas, and glories by use of Mie theory. *Appl. Opt.*, **42**, 436–444. [Available online at <http://www.philiplaven.com/index1.html>.]
- Lilly, D. K., and E. J. Zipser, 1972: The Front Range windstorm of 11 January 1972: A meteorological narrative. *Weatherwise*, **25**, 56–63.
- Lock, J. A., and L. Yang, 1991: Mie theory of the corona. *Appl. Opt.*, **30**, 3408–3414.
- Lynch, D. K., and W. Livingston, 2001: *Color and Light in Nature*. 2d ed. Cambridge University Press, 288 pp.
- Meinel, A., and M. Meinel, 1983: *Sunsets, Twilights, and Evening Skies*. Cambridge University Press, 163 pp.
- Mims, F. M., 1998: Solar corona caused by juniper pollen in Texas. *Appl. Opt.*, **37**, 1486–1488.
- Minnaert, M. J. G., 1954: *The Nature of Light and Colour in the Open Air*. Dover, 392 pp.
- , 1992: *Light and Color in the Outdoors* (Translated and revised by Len Seymour). Springer-Verlag, 417 pp.
- Parviainen, P., C. F. Bohren, and V. Makela, 1994: Vertical elliptical coronas caused by pollen. *Appl. Opt.*, **33**, 4548–4554.
- Platt, C. M. R., J. D. Spinhirne, and W. D. Hart, 1989: Optical and microphysical properties of a cold cirrus cloud: Evidence for regions of small ice particles. *J. Geophys. Res.*, **94**, 11 151–11 164.
- Pruppacher, H. R., and J. D. Klett, 1980: *Microphysics of Clouds and Precipitation*. Reidel Publishing, 714 pp.
- Queney, P., 1948: The problem of airflow over mountains: A summary of theoretical studies. *Bull. Amer. Meteor. Soc.*, **29**, 16–26.
- Ralph, F. M., P. J. Neiman, T. L. Keller, D. Levinson, and L. S. Fedor, 1997: Observations, simulations, and analysis of nonstationary trapped lee waves. *J. Atmos. Sci.*, **54**, 1308–1333.
- Sassen, K., 1979: Iridescence in an aircraft contrail. *J. Opt. Soc. Amer.*, **69**, 1080–1084.
- , 1991: Corona-producing cirrus cloud properties derived from polarization lidar and photographic analyses. *Appl. Opt.*, **30**, 3421–3428.
- , and G. C. Dodd, 1988: Homogeneous nucleation rate for highly supercooled cirrus cloud droplets. *J. Atmos. Sci.*, **45**, 1357–1369.
- , D. O. Starr, and T. Uttal, 1989: Mesoscale and microscale structure of cirrus clouds: Three case studies. *J. Atmos. Sci.*, **46**, 371–386.
- , G. G. Mace, J. Hallett, and M. R. Poellot, 1998: Corona-producing ice clouds: A case study of a cold mid-latitude cirrus layer. *Appl. Opt.*, **37**, 1477–1485.
- Shaw, J. A., and P. J. Neiman, 2003: Coronas and iridescence in mountain wave clouds. *Appl. Opt.*, **42**, 476–485.
- Simpson, G. C., 1912: Coronae and iridescent clouds. *Quart. J. Roy. Meteor. Soc.*, **38**, 291–299.
- Smith, R. B., 1979: The influence of the mountains on the atmosphere. *Advances in Geophysics*, Vol. 21, Academic Press, 87–230.
- Tape, W., 1994: *Atmospheric Halos*. Antarctic Research Series, No. 64, Amer. Geophys. Union, 143 pp.
- Trankle, E., and B. Mielke, 1994: Simulation and analysis of pollen coronas. *Appl. Opt.*, **33**, 4552–4562.
- Tricker, R. A. R., 1970: *Introduction to Meteorological Optics*. American Elsevier, 285 pp.
- Whiteman, C. D., 2000: *Mountain Meteorology: Fundamentals and Applications*. Oxford University Press, 355 pp.

